

25 **Abstract**

26 Latent and recurrent productive infection of long-living cells, such as neurons, enables
27 alphaherpesviruses to persist in their host populations. Still, the viral factors involved in these
28 events remain largely obscure. Using a complementation assay in compartmented primary
29 peripheral nervous system (PNS) neuronal cultures, we previously reported that productive
30 replication of axonally-delivered genomes is facilitated by PRV tegument proteins. Here, we
31 sought to unravel the role of tegument protein UL13 in this escape from silencing. We first
32 constructed four new PRV mutants in the virulent Becker strain using CRISPR/Cas9-mediated
33 gene replacement: (i) PRV Becker defective for UL13 expression (PRV Δ UL13), (ii) PRV where
34 UL13 is fused to eGFP (PRV UL13-eGFP) and two control viruses (iii and iv) PRV where VP16
35 is fused with mTurquoise at either the N-terminus (PRV mTurq-VP16) or C-terminus (PRV
36 VP16-mTurq). Live cell imaging of PRV capsids showed efficient retrograde transport after
37 axonal infection with PRV UL13-eGFP, although we did not detect dual-color particles.
38 Surprisingly, immunofluorescence staining of particles in mid-axons indicated that UL13 might
39 be co-transported with PRV capsids in PNS axons. Superinfecting nerve cell bodies with UV-
40 inactivated PRV Δ UL13 failed to efficiently promote escape from genome silencing when
41 compared to UV-PRV wild type and UV-PRV UL13-eGFP superinfection. However, UL13 does
42 not act directly in the escape from genome silencing, as AAV-mediated UL13 expression in
43 neuronal cell bodies was not sufficient to provoke escape from genome silencing. Based on this,
44 we suggest that UL13 may contribute to initiation of productive infection through
45 phosphorylation of other tegument proteins.

46 **Importance**

47 Alphaherpesviruses have mastered various strategies to persist in an immunocompetent host,
48 including the induction of latency and reactivation in peripheral nervous system (PNS) ganglia.
49 We recently discovered that the molecular mechanism underlying escape from latency by the
50 alphaherpesvirus pseudorabies virus (PRV) relies on a structural viral tegument protein. This
51 study aimed at unravelling the role of tegument protein UL13 in PRV escape from latency. First,
52 we confirmed the use of CRISPR/Cas9-mediated gene replacement as a versatile tool to modify
53 the PRV genome. Next, we used our new set of viral mutants and AAV vectors to conclude on
54 the indirect role of UL13 in PRV escape from latency in primary neurons and on its spatial
55 localization during retrograde capsid transport in axons. Based on these findings, we speculate
56 that UL13 phosphorylates one or more tegument proteins, thereby priming these putative proteins
57 to induce escape from genome silencing.

58

59 **Keywords**

60 Herpesvirus, alphaherpesvirus, pseudorabies virus, latency, PNS neurons

61

62 **Introduction**

63 Alphaherpesviruses, including herpes simplex virus (HSV-1 and -2), varicella zoster virus (VZV)
64 and pseudorabies virus (PRV), are ancient pathogens that have evolved with their hosts. Over the
65 years, these viruses have developed a remarkable way to persist in the host population: a lifelong
66 persistent infection, termed latency or quiescence, with periodic reactivation, in which the viral
67 genome re-enters productive replication (1). Productive replication occurs after a cascade-
68 dependent process of viral gene transcription followed by assembly of new progeny virions (2).
69 Productive replication is often accompanied by pathologies such as oral and genital ulcerations,
70 dermatomal rash with pain and itching, reproductive disorders like abortion and neonatal disease,
71 or nervous system disorders such as encephalitis (3). As far as is known, no pathologies are
72 directly associated with the latent infection. A hallmark of all alphaherpesviruses is the
73 establishment of latency in peripheral ganglia of the nervous system (e.g. the trigeminal ganglion)
74 after primary productive infection in mucosal epithelia. Remarkably, infected neurons do not die,
75 but rather the viral genome is stably retained in neuronal nuclei in absence of detectable viral
76 protein expression, rendering the infection undetectable by the immune system. However,
77 periodic reactivation and subsequent progeny virion production is essential for efficient
78 transmission of infection to new hosts. Reactivated virions travel back from neuronal bodies to
79 mucosae via anterograde axonal transport. Efficient replication in the epithelium promotes
80 shedding of infectious progeny virions in mucosal secretions which are available to infect new
81 hosts (1-3).

82 Despite the crucial role of latency and periodic reactivation in alphaherpesvirus persistence and
83 pathogenesis, the molecular mechanisms underlying these events are not well understood. O. O.
84 Koyuncu et al. (4) recently identified two different mechanisms for pseudorabies virus (PRV), a

85 swine alphaherpesvirus closely related to HSV-1 and -2, to escape from latency: (i) a cellular
86 stress-mediated slow route and (ii) a viral tegument-mediated fast route. The former route
87 involves cellular protein kinase A and c-Jun N-terminal kinase activity and has already
88 extensively been studied, while the latter acts independently from cellular kinases but the
89 mechanism remains obscure so far. These findings were discovered using an *in vitro* trichamber
90 model, in which peripheral neuron cell bodies are physically and fluidically separated from their
91 axonal termini (5). Administration of a low viral dose in the axonal compartment mimics the
92 natural route of neuronal invasion by long distance retrograde axonal transport. This protocol
93 results in the establishment of a quiescent, reactivatable infection in neuron cell bodies (6).
94 Interestingly, simultaneous delivery of a high dose of UV-inactivated or nucleocapsid-deficient
95 PRV particles to nerve cell bodies enabled infectious PRV genomes to escape from latency after
96 inoculation at the axonal compartment (4). These results implied that specific viral tegument
97 proteins are required to induce a productive viral infection in neurons. The researchers ruled out
98 the PRV early protein EP0, and the viral kinase Us3 (4). However, the exact viral tegument
99 protein or proteins responsible for PRV escape from genome silencing remain unknown. In this
100 context, HSV-1 tegument protein UL13 is known to promote viral transcription through
101 alterations in RNA polymerase II phosphorylation (7). UL13 is a serine/threonine kinase
102 conserved throughout all members of the *Herpesviridae* (8). Alternatively, this viral kinase might
103 activate specific cellular pathways or phosphorylate other viral tegument proteins, which in turn
104 may stimulate viral gene transcription.

105 The main objective of our study was to pinpoint the role of UL13 in the escape from PRV
106 genome silencing. Therefore, we constructed a PRV mutant that did not express UL13, and an
107 adeno-associated virus (AAV) vector expressing UL13 to determine if UL13 was necessary and

108 sufficient to induce PRV escape from genome silencing in neurons. In addition, we hypothesized
109 that upon entry of PRV virions in axons, nucleocapsids harboring the viral genome are
110 transported separately from viral tegument proteins that orchestrate the onset of viral genome
111 transcription. To test this hypothesis, we sought to track UL13 protein transport in axons along
112 with nucleocapsids. Therefore, we also constructed PRV mutants harboring fluorescently-tagged
113 UL13 or VP16 to track viral protein transport in axons via live-cell imaging. Tegument protein
114 VP16 is a viral transcription activator that is transported separately from PRV nucleocapsids in
115 chick embryo dorsal root ganglia (DRG) (9). All PRV mutants were constructed using
116 CRISPR/Cas9, one of the most powerful and versatile tools for precise gene editing at the present
117 time (10). The traditional approach to construct herpesvirus mutants involved homologous
118 recombination of DNA fragments with the viral genome, often introduced as a bacterial artificial
119 chromosome (BAC), which is a slow and laborious process. Genome engineering with
120 CRISPR/Cas9 relies on a single guide RNA (sgRNA) that directs an endonuclease (Cas9)
121 towards a specific gene locus due to sequence homology. The DNA at this locus is cleaved and
122 subsequently “repaired” by mammalian DNA repair mechanisms that are inherently error-prone,
123 thereby inducing insertions, deletions and mutations at the target site, potentially knocking out
124 expression of the specific gene product. Alternatively, foreign genes (e.g. fluorophore genes) can
125 be knocked-in through homologous recombination in presence of a DNA donor with homology
126 arms. Using this method, fluorophore-tagged viruses can be produced to facilitate screening. The
127 CRISPR/Cas9 toolbox has already been exploited for its gene editing potential in herpesviruses,
128 including herpes simplex virus (HSV), PRV and cytomegalovirus (CMV) (11-14). However, the
129 technology of editing functional PRV genes is still in development.

130 We first confirmed the use of CRISPR/Cas9 as an effective method to modify the PRV genome.
131 Following characterization of this newly constructed set of mutants, we confirmed that VP16 is
132 not co-transported with PRV nucleocapsids during retrograde axonal transport upon viral entry in
133 axons via live-cell imaging. The fluorescent signal of UL13-eGFP was too faint for live-cell
134 imaging, but immunofluorescence staining indicated that UL13 is co-transported with PRV
135 nucleocapsids during retrograde axonal transport. Finally, we demonstrated that UL13 is
136 indirectly involved in PRV genome escape from silencing.

137 **Materials and methods**

138 **Cells**

139 *Cell lines*

140 Porcine kidney epithelial cells (PK15; ATCC) were used to produce and titer PRV stocks. Human
141 embryonic kidney cells expressing large T antigen (HEK293T cells; ATCC) were used to
142 produce CRISPR lentiviruses, PRV mutants and adeno-associated viruses (AAVs). All cells were
143 maintained in Dulbecco's modified Eagle medium (DMEM) supplemented with 10% fetal bovine
144 serum, 1% penicillin and streptomycin (DMEM complete medium).

145 *Primary neurons*

146 Superior cervical ganglia (SCGs) were isolated from embryonic day 17 Sprague-Dawley rat
147 embryos (Hilltop Labs, Scottsdale, PA, USA) as previously described (15). SCG neurons were
148 cultivated either dissociated in plain dishes or compartmented in trichamber-mounted dishes.
149 Plastic tissue culture dishes (35 mm, Falcon[®]) or optical plastic dishes (Ibidi[®]) were coated with
150 500 µg/ml of poly-DL-ornithine (Sigma Aldrich) and 10 µg/ml of natural mouse laminin
151 (Invitrogen). Trichambers were installed onto these dishes for compartmentation of neurons and
152 axons as previously described (5). Neurons were cultured for a minimum of 4 weeks prior to
153 experiments.

154 *Viruses*

155 PRV Becker is a wild-type (PRV WT) strain commonly used as background for PRV mutants
156 (16). PRV 180 expresses a monomeric red fluorescent protein (mRFP)-VP26 fusion protein in a
157 PRV Becker background (17). PRV Δ UL13, PRV 180 eGFP-UL13, PRV 180 mTurq-VP16 and
158 PRV 180 VP16-mTurq viruses were constructed using CRISPR/Cas9-mediated gene
159 replacement, as described below.

160 **Plasmids and sgRNA selection**

161 Synthesized oligo primers (Integrated DNA Technologies, Coralville, IA, USA) corresponding to
162 separate targets were cloned into an EspI-digested (New England Biolabs, Ipswich, MA, USA)
163 LentiCRISPR v2 plasmid (gift from Feng Zhang; Addgene plasmid #52961). Guide sequences
164 were selected using CRISPOR by containing minimal mismatches to any human or PRV genomic
165 sequences, while maximizing their presumable on target effect (18). Selected target sites and
166 PAM sequences are shown in Table 1. There were no potential off-target regions in the PRV
167 genome, as determined using CRISPOR (<http://crispor.tefor.net/>) (19).

168 Donor plasmids were constructed using the HiFi DNA assembly method (New England Biolabs)
169 as described below. All donor plasmids consisted of a pcDNA3-eGFP backbone (gift from Doug
170 Golenbock; Addgene plasmid # 13031), an upfront and downstream homology arm with eGFP or
171 mTurquoise in between (Fig. 1B). Each set consisted of four fragments, which were PCR-
172 amplified from purified PRV DNA (homology arms), pcDNA3-eGFP (vector backbone and
173 eGFP) or pcDNA3-mTurq (mTurquoise v2) using Q5 high-fidelity polymerase (New England
174 Biolabs) and specific primer pairs shown in Table 2 (Integrated DNA Technologies). Silent
175 mutations (underlined) were introduced in PAM sequences of PRV 180 fusion mutants.

176 The backbones of AAV plasmids (CMV-eGFP-p2a-WPRE-SV40pA or CMV-eGFP-p2a-UL13-
177 WPRE-SV40pA) were generated by cloning. Purified viral DNA, a pAAV-mTurq-p2a-WPRE-
178 SV40pA (Engel lab) and pcDNA-eGFP vector were modified by PCR and assembled using HiFi
179 DNA assembly (NEB). Specific fragments and primer pairs are shown in Table 2.

180 **Lentivirus production and transduction**

181 Lentiviruses were produced in HEK293T cells by co-transfecting LentiCRISPRv2 plasmids
182 containing separate targets with packaging plasmids pMD2.G and psPAX2 using PEI reagent
183 (VWR International, Radnor, PA, USA) at a DNA:PEI ratio of 1:3 (w/w) following a chloroquine
184 hydrochloride (25 μ M; Sigma-Aldrich, St. Louis, MO, USA) pre-incubation step. Fifty-six hours
185 post transfection, cell supernatant was collected, centrifuged at 900 g, clarified by passing
186 through a 0.45 μ m PES filter and stored at -80°C. Lentiviral titers were determined using the
187 QuickTiter™ Lentivirus Titer Kit according to the manufacturer's instructions (Cell Biolabs, San
188 Diego, CA, USA).

189 Fresh HEK293T cells were transduced for 48 h with CRISPR lentiviruses at a MOI of 2.5 in the
190 presence of 10 μ g/mL polybrene (Sigma-Aldrich). After 48 h, medium was replaced daily by
191 fresh DMEM medium containing 10 μ g/mL puromycin for 5 days. Stably transfected cells were
192 then expanded and maintained in DMEM medium containing 5 μ g/mL puromycin. Monoclonal
193 cell lines (HEK293T-UL13sgRNA, HEK293T-VP16sgRNA1 and HEK293T-VP16sgRNA2)
194 were generated by limiting dilution in order to maintain a stable expression of sgRNAs and Cas9.
195 Briefly, 100 μ L of a cell suspension of 5 cells/mL was seeded into each well of a 96-well plate.
196 After 7 days of incubation, the wells were visually inspected for colony formation. Wells
197 harboring only 1 colony were selected, while those without or with 2 or more colonies were
198 discarded. After full expansion, Cas9 expression was evaluated using the Cas9 ELISA kit of Cell

199 Biolabs according to the manufacturer's instructions. Monoclonal cell lines expressing between
200 150 and 200 ng/mL Cas9 were selected for downstream experiments.

201 **Adeno-associated virus production**

202 AAV plasmids containing either CMV-eGFP-p2a-WPRE-SV40pA or CMV-eGFP-p2a-UL13-
203 WPRE-SV40pA were packaged into AAV-PHP.eB capsids (gift from Viviana Gradinaru,
204 Addgene plasmid #103005) at the Princeton Neuroscience Institute Viral Core Facility (20).
205 AAV particles were purified by iodixanol step gradient followed by column ultrafiltration as
206 previously described (21, 22). Infectious viral genomes were measured by Taq-Man qPCR.

207 **CRISPR/Cas9-mediated gene editing**

208 HEK293T-UL13sgRNA and HEK293T-VP16sgRNA1 and HEK293T-VP16sgRNA2 cells were
209 pre-treated with chloroquine hydrochloride prior to transfection with mock plasmids or donor
210 plasmids using PEI reagent as described above. After 24 h, cells were inoculated with either
211 mock, PRV WT or PRV 180 at a MOI of 1. Cells were further maintained in DMEM complete
212 medium supplemented with 10 μ M SCR7 and 10 μ M RS-1 (Sigma-Aldrich) to inhibit non-
213 homologous end joining and enhance homologous recombination, respectively. Forty-eight hours
214 post inoculation, cells and supernatant were harvested, pooled and stored at -80°C. Viral stocks
215 were titrated on PK15 cells using classic plaque assay and screened for eGFP or mTurquoise
216 expression by immunofluorescence microscopy. Fluorescent plaques were subjected to 3 rounds
217 of plaque purification before propagating viral stocks on PK15 cells.

218 **(q)PCR analysis and sequencing**

219 Viral DNA was purified from different PRV stocks using QIAamp MinElute Virus Spin Kit
220 (Qiagen, Hilden, Germany) according to the manufacturer's instructions. UL13 and VP16 gene
221 regions were amplified using primer pairs UL13 seq and VP16 seq (Table 3) using Q5 high

222 fidelity polymerase (New England Biolabs) in the presence of 4% DMSO (Sigma-Aldrich) and
223 2.5M Betaine (Sigma-Aldrich). Sequences were confirmed by Sanger sequencing (Genewiz,
224 South Plainfield, NJ, USA).

225 Genome copies per mL were determined for each virus stock by means of quantitative PCR
226 (qPCR). Virus stocks were first treated with 100 U of DNase I for 30 min at 37°C
227 (ThermoFisher) followed by inactivation for 10 min at 80°C. Samples were then digested with
228 proteinase K (New England Biolabs) in 0.5% Tween 20 for 60 min at 55°C, followed by
229 inactivation for 10 min at 95°C. Viral genomic DNA was quantified by using UL54-specific
230 primers (Table 3), as previously published (23). A serial dilution of purified whole genome of
231 PRV Becker virions functioned as standard. Triplicate reaction mixtures were prepared using a
232 KAPA SYBR[®] FAST qPCR kit (Sigma-Aldrich). Each experiment was performed in duplicates.
233 The qPCR was performed with an Eppendorf RealPlex Mastercycler with the following
234 amplification conditions: preincubation at 95° for 2 min with 40 cycles of denaturation (5 s at
235 95°C), annealing (20 s at 55°C), and extension (10 s at 72°C). The quantification cycle (CT)
236 values were calculated using Mastercycler EP RealPlex 2.2 software. Sample CT values were
237 plotted against standard dilution values to determine exact genomic DNA concentrations. Finally,
238 DNA concentrations were converted into viral genome copies/mL based on the total PRV
239 genome size (141,113 bp).

240 **Virus purification**

241 Culture supernatants of PRV-infected PK15 cells were clarified by centrifugation at 40,000 g for
242 30 min at 4°C. The virion pellet was pooled onto a discontinuous OptiPrep[™] gradient (Sigma-
243 Aldrich) containing 10-30% (w/v) of iodixanol and centrifuged at 100,000 g for 2.5 h at 4°C.
244 After centrifugation, purified opalescent virion bands were harvested at the interface of the 15%

245 and 20% layers. Virion bands were pooled in HNE buffer (5 mM HEPES, 150 mM NaCl, 0.1
246 mM EDTA, pH 7.4) by the use of a 50K filter device (Millipore corporation, Bedford, MA,
247 USA).

248 **Compartmented complementation assay in primary neurons**

249 SCG neurons were infected by adding low MOI ($10^{2.5}$ PFU) PRV 180 to the axonal (N)
250 compartment to enable genome silencing after axonal transport. UV-inactivated PRV WT or
251 mutants (10^{10} genome copies $\sim 10^{5-6}$ PFU) were added at the same time in the S compartment. We
252 chose to standardize for genome copies instead of PFU, as PRV mutant stocks might contain
253 more non-infectious virus particles compared to PRV WT. These defective particles might still be
254 capable of delivering their content (e.g. tegument proteins) to neurons, thereby biasing the results.
255 AAVs were added 3 days prior to PRV inoculation to ensure stable UL13 and/or eGFP
256 expression, but no overexpression, prior to inoculation.

257 **Virus plaque assay**

258 PK15 cells were grown to confluency in 6-well dishes prior to inoculation with 10^6 genome
259 copies (~ 10 -100 PFU) of PRV WT or PRV mutants for 1 h at 37°C. Next, cells were covered
260 with a solution containing 50% 2 \times MEM (Thermo Fisher Scientific) and 50% 1.88%
261 carboxymethylcellulose (Sigma-Aldrich). Forty-eight hours post inoculation (hpi), media was
262 removed, and cells were fixed in ice-cold methanol for 20 min at -20°C. To visualize virus
263 plaques and/or single infected cells, viral immediate early (IE) 180 protein was stained for
264 immunofluorescence as described below using a rabbit polyclonal anti-IE180 protein antibody
265 and Alexa Fluor 488-conjugated goat anti-rabbit antibodies (24).

266 **Viral growth kinetics**

267 PK15 cells were grown to confluency in 24-well dishes and dissociated SCGs were cultivated for
268 4 weeks on optical plastic dishes prior to inoculation. Cells were inoculated with PRV WT or
269 mutants at a MOI of 1 for 1 h at 37°C. Next, cells were briefly exposed to 40 mM citrate buffer
270 (pH 3) to inactivate any free virus particles left from the inoculum that had not infected. After 3
271 washing steps with DMEM, cells were further incubated with complete medium at 37°C. At
272 indicated time points, supernatants were collected for virus titration and cells were fixed in ice-
273 cold methanol (20 min at -20°C) for immunofluorescence staining.

274 **Virus titration**

275 PRV titrations were conducted on PK15 cells, which were incubated at 37 °C for 7 days. Titers
276 were expressed as TCID₅₀.

277 **Immunofluorescence staining**

278 *Purified virus particles*

279 For immunofluorescence staining of purified virus particles, one µL of purified virus stocks was
280 spotted onto glass coverslips and left to adsorb to the glass for 15 min at 37°C. Particles were
281 permeabilized in 0.1% Triton X-100 followed by 1 h staining at 37°C with primary antibodies
282 (rabbit anti-UL13 antibody, produced in house, rabbit anti-VP16 antibody, produced by
283 GenScript [Piscataway, New Jersey, USA] or isotype control rabbit IgGs against rabies virus
284 nucleoprotein (25)) diluted in phosphate-buffered saline (PBS) with 10% normal goat serum
285 (NGS) and Alexa Fluor 647-conjugated secondary antibody (Thermofisher). Particles were
286 washed 3 times with PBS for 5 min per wash prior to and after secondary antibody staining.

287 *Viral growth kinetics in PK15 cells and SCG neurons*

288 For immunofluorescence staining of infected PK15 cells and dissociated SCGs, cells were fixed
289 in methanol at -20°C for 20 min at the indicated times after infection. Primary antibodies (rabbit
290 polyclonal anti-UL13, rabbit polyclonal anti-VP16, rabbit polyclonal anti-VP26, mouse
291 monoclonal anti-U_s3 and isotype controls (26)) were diluted in 10% NGS-PBS and added to cells
292 for 1 h at 37°C followed by incubation of 1 h at 37°C with Alexa Fluor 488 (green)-, 594 (red)-
293 or 647 (magenta)-conjugated secondary antibodies. During the last 10 min of secondary antibody
294 staining, DAPI was added to cells to stain cell nuclei.

295 *Chambered SCG neurons*

296 For immunofluorescence staining of chambered SCGs during virus trafficking experiments, cells
297 were fixed in 1% PFA at room temperature (RT) for 10 min, permeabilized in 0.1% Triton X-100
298 for 2 min at RT. Staining was performed with primary polyclonal rabbit anti-eGFP antibodies
299 (Invitrogen) or isotype control antibodies and secondary Alexa Fluor 488-conjugated antibodies,
300 as described above.

301 **(Live-cell) imaging**

302 All imaging was done using a previously described Nikon Ti-E inverted epifluorescence
303 microscope (27).

304 *Virus particle trafficking*

305 Virus particle trafficking was assessed using live-cell imaging as described previously (28).
306 Briefly, chambered SCGs grown onto Ibidi glass dishes were placed inside a stage top incubator
307 system at 37°C and 5% (v/v) CO₂ (Live Cell Instrument/Quorum Scientific), prior to inoculation
308 with 10⁶ PFU of virus. Movies were acquired either with phase, green, red and cyan fluorescence
309 filters using a 60× Plan Fluor Ph3 objective (Nikon) and an iXon 895 back-thinned electron

310 multiplying charge-coupled device (EM-CCD) camera (Andor, Belfast, Northern Ireland). The
311 imaging window was maintained at a fixed height of 100 pixels and width of 300 pixels. The
312 fluorescence exposure was set to 200 ms, with the EM Gain filter set to 300. The acquisition rate
313 was approximately 4 frames per second, on average. For the dual fluorescent movies, the
314 exposure was set to 300 ms and the acquisition rate was approximately 1 frame per second.
315 Movies were created and virus particles were manually tracked in infected axons using ImageJ
316 software (National Institute of Health, Bethesda, MD, USA).

317 *Escape from silencing*

318 Escape from silencing was assessed on tiled images of the entire S compartment. These images
319 were captured using Nikon NIS Elements software, a Cool Snap ES2 camera (Photometrics), and
320 4x magnification objective (Nikon). Color thresholds were set manually, prior to converting
321 images to 8-bit grey-scale images using ImageJ. Next, the relative amount of red fluorescence
322 (viral production) was divided by the amount of green fluorescence (only those neurons that
323 project their axons to the N compartment) to determine the percentage of susceptible neurons that
324 escape from silencing. Since the majority of neurons sent axons through the N compartment
325 (>90%), only the percentage of red fluorescence was monitored (viral production) upon AAV
326 inoculation.

327 *Co-localization image analysis*

328 Co-localization of red (capsids) and green/cyan (UL13/VP16) puncta was verified by image
329 analysis using ImageJ. Briefly, RGB images were converted to 8-bit images and subjected to
330 conservative thresholding. Next, binary image multiplication was used to determine the overlap
331 of puncta. The results of 5 microscopic fields were added to obtain a total value.

332 Co-localization of UL13 with eGFP, and VP16 with mTurquoise, respectively, in infected cells
333 was verified by image analysis using ImageJ. Briefly, RGB images were converted to 8-bit
334 images. Next, binary image subtraction was used to determine the overlap of colors.

335 **Western blot analysis**

336 Virion protein content of newly constructed PRV mutants was characterized by Western blot
337 analysis. For this, 10^{12} genome copies of purified virus stocks were mixed with 5x Laemmli
338 buffer and heated at 95°C for 5 min. Samples were then loaded onto 10% NuPAGE BisTris gels
339 (Invitrogen) and run for 15 min at 100V and 45 min at 200V in MOPS buffer. Proteins were
340 transferred to nitrocellulose membranes using semidry transfer at 18V for 90 min. Next,
341 membranes were washed 2 times with ultrapure water for 2 min and incubated in antigen
342 pretreatment solution (Invitrogen) for 10 min at RT. After 5 rinses with ultrapure water,
343 membranes were incubated in 5% non-fat dry milk in phosphate-buffered saline supplemented
344 with 0.1% Tween 20 (PBST) solution for 1 h at RT. Following three 5 min washing steps in
345 PBST, membranes were stained with primary antibodies diluted 1:1,000 in primary antibody
346 diluent (Invitrogen) overnight at 4°C. Secondary antibodies (goat anti-mouse or –rabbit
347 antibodies conjugated to horseradish peroxidase [ThermoFisher Scientific]) were diluted
348 1:20,000 in 1% milk-PBST solution and added to the membranes for 30 min at RT after and prior
349 to a thorough washing step (4 times 5 min washing in PBST). Membranes were incubated with
350 chemiluminescent substrates (Supersignal Dura, ThermoFisher scientific). Protein bands were
351 visualized by exposure on HyBlot CL (Denville scientific) blue X-ray films. Primary antibodies
352 used for Western blot: anti-VP5 mouse monoclonal antibody (mAb) (gift of H. J. Rziha, Federal
353 Research Center for Viruses Diseases for Animals, Tübingen, Germany), anti-Us3 mouse mAb
354 (26), anti-UL13 polyclonal rabbit sera (produced in-house). VP5 (capsid) protein functioned as

355 internal loading control to determine relative amount of proteins present in different purified
356 virus stocks. This was determined through plot profiling in ImageJ.

357 **Statistical analyses**

358 Significant differences ($P < 0.05$) between different CRISPR-gene editing methods or between
359 mock- or different PRV mutant-inoculated cells were identified by analysis of variance
360 (ANOVA), followed by a Tukey post-hoc test. If homoscedasticity of the variables was not met,
361 as assessed by Levene's test, the data were log transformed prior to ANOVA. The normality of
362 the residuals was verified using the Shapiro-Wilk test. If the variables remained heteroscedastic
363 or normality was not met after log transformation, a Kruskal-Wallis test, followed by Mann-
364 Whitney's post hoc test, was performed. All analyses were conducted in IBM SPSS Statistics for
365 Windows, version 25.0 (IBM Corp., Armonk, NY, USA).

366 **Ethics statement**

367 All animal work was performed in accordance with the Princeton Institutional Animal Care and
368 Use Committee (protocols 1947–16). Princeton personnel are required to adhere to applicable
369 federal, state, local and institutional laws and policies governing animal research, including the
370 Animal Welfare Act and Regulations (AWA); the Public Health Service Policy on Humane Care
371 and Use of Laboratory Animals; the Principles for the Utilization and Care of Vertebrate Animals
372 Used in Testing, Research and Training; and the Health Research Extension Act of 1985.

373 **Data availability statement**

374 The raw data supporting the conclusions of this manuscript will be made available by the authors,
375 without undue reservation, to any qualified researcher.

376

377 **Results**

378 **CRISPR/Cas9 is an effective tool to edit PRV genomes**

379 Different PRV mutants were constructed using CRISPR/Cas9-mediated homologous
380 recombination, as schematically shown in Fig. 1A and B.

381 PRV null for UL13 protein expression (PRV Δ UL13) was constructed from a PRV wild type
382 (WT) Becker strain background by replacing the mid-part of UL13 coding sequence (CDS) with
383 the eGFP coding sequence. Both ends of the UL13 CDS were left intact, as they overlap with
384 those of UL12 and UL14. A UL13-eGFP fusion mutant was constructed in a PRV 180
385 background. PRV 180 is a virus previously made to express red-fluorescent capsid to allow for
386 imaging of individual viral particles in living neurons (17, 29). Enhanced GFP (eGFP) was
387 inserted at position 105 of UL13, as it could not be fused to UL13 N- or C-terminus without polar
388 effects on UL12 and UL14. Both PRV UL13 mutants were produced in a HEK293T cell line
389 expressing Cas9 and UL13 sgRNA (Table 1) targeting the inner region of UL13.

390 VP16 is abundantly present in the PRV tegument and has already been visualized during
391 transport in axons (9). Accordingly, we fused PRV 180 VP16 to the fluorophore mTurquoise
392 version 2 (mTurq) to serve as internal control for transport. The coding sequence of VP16 and its
393 flanking regions do not overlap with those of other proteins and thus, mTurquoise v2 could be
394 linked to either N- (mTurq-VP16 PRV180) or C-termini (VP16-mTurq PRV180) of VP16. The
395 former and latter were constructed in HEK293T monoclonal cell lines stably expressing Cas9 and
396 VP16 sgRNA1 or sgRNA2, respectively (Fig. 1A).

397 First, we assessed the efficacy of viral mutant production using homologous recombination
398 induced by CRISPR/Cas9 by comparing the amount of fluorescent virus produced in control

399 HEK293T cells with monoclonal HEK293T cell lines expressing different sgRNAs and Cas9
400 (Fig. 1C). Although transfection of 10 μ g of whole PRV genomes in control HEK293T cells
401 resulted in production of 10^3 PFU/mL progeny virus, sgRNA/Cas9-expressing HEK293T cells
402 did not support any detectable viral replication upon transfection of viral DNA (<10 PFU/mL). In
403 contrast, infection with intact PRV virions (MOI of 1) consistently resulted in efficient viral
404 progeny production with titers ranging from 10^6 to 10^7 PFU/mL in all different cell types. In
405 absence of donor plasmids containing the fluorophore flanked by homology arms, no fluorescent
406 plaques were observed upon assay of progeny virus. However, addition of donor plasmids,
407 followed by PRV inoculation resulted in the production of fluorophore-harboring progeny viruses
408 with the highest efficacy (>80% of fluorescent plaques) observed for the VP16-mTurq fusion
409 mutant. These results show that CRISPR/Cas9 is a simple and effective way to produce PRV
410 mutants.

411 **Confirmation of CRISPR/Cas9-constructed PRV mutants**

412 Mutations were confirmed through PCR amplification followed by Sanger sequencing,
413 immunofluorescence (staining) and Western blot analysis.

414 First, correct insertion of fluorescent protein genes into the genome of plaque-purified PRV
415 mutants was analyzed. DNA of purified virus stocks was first subjected to PCR using region-
416 specific primers (Table 3). Identities were then confirmed by Sanger sequencing. Next,
417 fluorophore expression was evaluated after infection with different PRV mutants. Infection of
418 PK15 cells with PRV Δ UL13 lead to significant green fluorescence, compared to cell infection
419 with PRV WT (Fig. 2A). PK15 cells infected with double-tagged PRV 180 UL13-eGFP emitted
420 green fluorescence in addition to red fluorescence, while PRV 180-infected PK15 cells only
421 emitted red fluorescence (Fig. 2B). Interestingly, UL13-eGFP mainly accumulated around the

422 nucleus (perinuclear region) of PK15 cells, as depicted by the magnified image in the lower right
423 corner of Fig. 2B. Likewise, double tagged PRV 180 mTurq-VP16 and PRV 180 VP16-mTurq
424 induced the formation of double cyan and red fluorescent viral plaques. Viral plaque assays
425 consistently showed that all viral mutant plaques emitted the correct fluorescent signals, showing
426 that there was no contamination of parental viral strains.

427 Correct protein expression of different PRV mutants was confirmed by double
428 immunofluorescence staining of PK15 cells infected with different PRV viruses, as shown in Fig.
429 2C and D. PRV WT-infected PK15 cells clearly expressed UL13, while PRV Δ UL13-infected
430 cells did not (Fig. 2C). In Fig. 2D, co-localization analysis in ImageJ of PRV fusion mutants
431 shows perfect overlap between UL13 and eGFP in PRV UL13-eGFP (upper panels) and between
432 VP16 and mTurquoise in PRV 180 mTurq-VP16 and PRV 180 VP16-mTurq (lower panels).

433 Western blot analysis of purified extracellular virions (10^{12} genome copies) was performed to
434 assess structural incorporation of different proteins into PRV virions. Staining of major capsid
435 protein VP5 functioned as loading control to correlate protein expression to the amount of capsid
436 protein. Analysis of UL13 demonstrates absence of UL13 in PRV Δ UL13, compared to PRV WT
437 (red arrow). As expected, the UL13-positive band of PRV UL13-GFP had shifted to ± 75
438 kilodaltons (kDa) from ± 40 kDa for PRV 180 due to fusion with eGFP (± 27 kDa). The purple
439 arrows indicate a nonspecific band present in all purified PRV strains. Absence of UL13 kinase
440 activity could result in excessive incorporation of another important viral kinase, Us3. However,
441 equal relative amounts of Us3 were present between PRV WT and PRV Δ UL13, when
442 normalized to the major capsid protein VP5. While VP16 expressed from PRV WT and from
443 PRV Δ UL13 was present as a single protein band, VP16 of PRV 180 and PRV 180 UL13-GFP
444 was present as a double band. This intriguing phenomenon was also apparent on gel

445 electrophoresis of PCR-amplified products of the VP16 region of the respective viruses (Fig 2E
446 and primers are shown in Table 3). This suggests that during production of PRV 180, mutations
447 such as duplications occurred in PRV 180 genome, resulting in multiple gene transcripts and thus
448 protein bands. For VP16 of PRV 180 VP16-mTurq and PRV 180 mTurq-VP16 virions, a triple
449 band was documented. The upper band of ± 75 kDa corresponds to the fusion protein consisting
450 of VP16 (± 50 kDa) and mTurquoise (± 27 kDa).

451 **Characterization of CRISPR/Cas9-constructed PRV mutant infection in PK15 cells and** 452 **dissociated SCG neurons**

453 Virus plaque formation was assessed in PK15 cells by standardizing the inoculum at 10^6 genome
454 copy numbers per PRV mutant (Fig. 3A). Deletion of UL13 in PRV WT resulted in a significant
455 reduction of 82.7 ± 0.3 % in viral plaque formation, showing that PRV Δ UL13 is less capable of
456 infecting PK15 cells. In addition, the average size of PRV Δ UL13 plaques was significantly
457 smaller (742 ± 135 μ m) when compared to that of PRV WT (958 ± 166 μ m), pinpointing the
458 importance of UL13 in viral spread. Although in a plaque assay comparing stocks with equivalent
459 numbers of genomes, PRV 180 formed significantly fewer plaques compared to PRV WT, no
460 significant difference was observed in the number of plaques or plaque diameters between PK15
461 cells inoculated with different PRV 180 or different PRV 180 fusion mutants. This indicates that
462 UL13 or VP16 fusion proteins do not interfere with the ability of PRV virions to infect PK15
463 cells.

464 Kinetics of viral protein expression and virus propagation were assessed in PK15 cells by
465 standardizing the inoculum at a MOI of 1. As shown in the Fig. 3B, all viral mutants grew less
466 well when compared to PRV WT, as shown in the reduction of virus titers. However, between
467 PRV 180 and different PRV 180 fusion mutants, no overall significant difference was observed in

468 viral titers. Temporal expression of IE180, Us3, gB or VP26 did not significantly differ between
469 the parental strains and different viral mutants (Fig. 3C). Except for PRV Δ UL13, which lacked
470 UL13 expression, all viruses started expressing UL13 at similar time points. The number of cells
471 expressing VP16 did not differ between parental strains (PRV WT and PRV 180) and their
472 derivatives (PRV Δ UL13 and PRV 180 UL13-eGFP, PRV 180 mTurq-VP16 or PRV 180 VP16-
473 mTurq, respectively). However, all PRV 180 strains had a lower percentage of VP16-positive
474 cells between 3 and 9 hpi compared to PRV WT and PRV Δ UL13, which might reflect mutations
475 in the genome of PRV 180, as suggested by the multiple VP16 transcripts and proteins expressed
476 by PRV 180, when compared to PRV WT. Finally, we evaluated infection of dissociated SCG
477 neurons by different PRV mutants. No significant difference was observed among different
478 viruses upon infection at MOI 1. Indeed, all neurons were positive for IE180 at 3 hpi and at 9 hpi,
479 all neurons expressed PRV late proteins UL13, VP16 and VP26. Still, no virus replication was
480 observed in dissociated SCG neurons, as viral titers in cell supernatant remained undetectable.

481 Since there was no significant difference in the different infectivity parameters between N- or C-
482 terminal tagging for the mTurq-labelled VP16 PRV 180 mutants, further experiments were
483 conducted with the N-terminal variant only.

484 **UL13, but not VP16, is co-transported with PRV capsids in SCG neurons**

485 Our newly constructed collection of dual fluorescent PRV mutants was used to track PRV
486 capsids along with tegument proteins UL13 or VP16 during live axonal transport in chambered
487 SCG neurons. To determine suitability of mutants in live-cell imaging, purified virus particles
488 were first spotted onto coverslips and fluorescence was verified. We observed red, as well as
489 cyan fluorescent puncta in the PRV 180 mTurq-VP16 stock, but we were unable to detect green
490 fluorescent puncta in the PRV 180 UL13-eGFP stock (Fig. 4 upper panel). This result suggests

491 that the amount of UL13-eGFP by itself was likely too low to emit detectable levels of green
492 fluorescence. However, immunofluorescence staining of eGFP confirmed that 82% of mRPF1-
493 capsid containing particles had incorporated UL13-eGFP (Fig. 4 middle panel). In the mTurq-
494 VP16 virus stock, 76% of red puncta co-localized with and cyan puncta, suggesting that the
495 majority of mRPF1-capsid containing particles in the virus stock had incorporated detectable
496 mTurq-VP16 (Fig. 4 lower panel).

497 Next, we performed live-cell imaging of moving virus particles in SCG axons. Starting from 30
498 min after inoculation in the N compartment, mRFP1-labelled capsids of PRV 180 dual
499 fluorescent strains were readily detected moving retrogradely (toward the cell bodies) in SCG
500 axons with dynamics similar to that of mono fluorescent PRV 180. Indeed, there was no
501 significant difference in the percentage of moving capsids between PRV 180 (79.29 ± 7.00 %),
502 PRV 180 UL13-eGFP (72.67 ± 8.55 %) and PRV 180 mTurq-VP16 (73.34 ± 10.87 %) (pie charts
503 of Fig. 5A). Further, the average velocity of capsid transport did not significantly differ between
504 PRV 180 (1.17 ± 0.55 $\mu\text{m/s}$), PRV 180 UL13-eGFP (1.07 ± 0.48 $\mu\text{m/s}$) and PRV 180 mTurq-
505 VP16 (1.14 ± 0.42 $\mu\text{m/s}$), as shown in Movie 1-3 and the graph of Fig. 5A. These findings show
506 that tagging UL13 or VP16 with a fluorophore does not influence transport dynamics of mRPF1-
507 capsids of PRV 180. During retrograde transport, only 4.34 ± 3.22 % of moving PRV 180
508 mTurq-VP16 capsids (red) emitted cyan fluorescence, while the majority of stationary particles
509 (78.41 ± 6.98 %) emitted red as well as cyan fluorescence.

510 Live cell imaging of UL13 was not possible due to low green fluorescence emission. Therefore,
511 axons in both the M and N compartment were fixed 2 hpi and stained for eGFP to track UL13
512 localization (Fig. 5B). It should be noted that fixation caused a decrease in mRFP fluorescence
513 and made it impossible to directly stain UL13 using our polyclonal rabbit serum. Still, staining

514 eGFP enabled us to detect UL13-eGFP. Interestingly, the percentage of red capsid puncta
515 colocalizing with green puncta was similar in the N compartment (75.51 ± 8.77 %), as in the M
516 compartment (80.69 ± 11.57 %). These data indicate that UL13 is co-transported with PRV
517 capsids during retrograde transport, while VP16 stays behind upon infection of neuronal axons.

518 **UL13 is involved indirectly in PRV escape from genome silencing in SCG neurons**

519 Using a trichamber neuron culture system, we previously showed that delivery of a high dose of
520 UV-treated or nucleocapsid-deficient PRV light (L) particles to neuronal cell bodies triggers
521 escape from silencing of infectious PRV viruses applied to axons, suggesting that tegument
522 proteins might be involved (4). To understand whether the viral kinase tegument protein UL13
523 plays a role, we applied 10^{10} genome copies of UV-inactivated PRV Δ UL13 virions to neuron
524 cell bodies, while simultaneously inoculating axons with low dose ($10^{2.5}$ PFU) red capsid-labelled
525 PRV 180 (Fig. 6A). Dioctadecyloxycarbocyanine perchlorate (DiO) was added to the N
526 compartment to identify neuronal cell bodies with axons that penetrate into the N compartment.
527 Phase and fluorescent images are shown in Fig. 6B. As expected, 86.3 ± 13.6 % of DiO-positive
528 (i.e. connected with N-compartment) neurons produced red fluorescence, corresponding to
529 mRPF1-capsid proteins, 4 dpi upon treatment with UV-inactivated PRV WT virions (Fig. 6C).
530 This percentage was significantly ($P < 0.05$) higher when compared to mock treatment (2.5 ± 3.8
531 %) or treatment with UV-inactivated PRV Δ UL13 (5.3 ± 8.3 %). Interestingly, we observed
532 similar results when standardizing the inoculum of UV-inactivated viruses for PFU (10^6 PFU),
533 even though neuronal cell bodies are flooded with defective viral particles delivering virion
534 proteins in case of UV-inactivated PRV Δ UL13, compared to PRV WT. Fusion of UL13 to eGFP
535 did not influence its function in escape from genome silencing, as indicated by the high

536 percentage of connecting neurons that escaped from silencing upon treatment with UV-
537 inactivated PRV 180 UL13-eGFP (88.0 ± 13.3 %).

538 To confirm the role of UL13 in PRV escape from genome silencing, we produced AAVs that
539 induce the expression of UL13 and reporter protein eGFP linked by self-cleavable p2a in SCG
540 neurons. AAVs expressing only p2a and eGFP functioned as controls. Neuronal cell bodies
541 started to express eGFP 2-3 dpi by AAVs, which accumulated over the following days. SCG
542 neurons clearly express UL13 6 dpi with AAV-UL13, as demonstrated by immunofluorescence
543 staining in Fig. 7A. Expression of UL13 did not influence cell viability, as analyzed using
544 ReadyProbes™ Cell Viability Imaging Kit (ThermoFisher Scientific). In contrast to UV-
545 inactivated PRV WT, UL13-expressing neurons were not sufficient to facilitate PRV 180
546 genomes to escape from silencing after inoculation of axons (Fig. 7B and C). Instead, only $3.6 \pm$
547 4.2 % of connecting neurons produced mRFP1-labelled capsid proteins in the presence of UL13
548 expression 4 dpi, showing that UL13 does not play a direct role in the escape from genome
549 silencing by PRV. Similarly, expression of eGFP or mock treatment of neurons did not induce
550 escape from genome silencing by PRV. Together, these data show that UL13 plays an indirect
551 role in the escape from genome silencing by PRV.

552 **Discussion**

553 Induction and escape from viral genome silencing in peripheral nervous system (PNS) neurons is
554 a hallmark of alphaherpesvirus biology. The dsDNA from incoming virions either rapidly
555 associates with histones resulting in genome silencing or is bound by RNA polymerase II to
556 initiate the orderly cascade of viral gene transcription followed by virion production. Still, the
557 exact molecular events that determine the fate of these incoming viral genomes are poorly
558 understood. Using a compartmented complementation assay in trichambers, O. O. Koyuncu et al.

559 (4) identified a new distinct molecular mechanism to start productive infection from quiescently
560 destined PRV genomes: a rapid viral tegument-mediated route. For example, complementing
561 neuronal cell bodies infected with UV-inactivated whole virions or light particles (contain
562 tegument proteins but lack nucleocapsids) facilitates productive axonal PRV 180 infection which
563 was destined to be silenced. In the current study, we sought to identify the role of the viral kinase
564 and tegument protein UL13 in the escape from PRV genome silencing in SCG neurons. This
565 study required the construction of new PRV mutants. Although some PRV Δ UL13 mutants have
566 been constructed in other PRV backgrounds, no PRV Becker Δ UL13 mutants without any other
567 modifications had been constructed (29, 30). As the Becker strain efficiently induces escape from
568 genome silencing, we constructed a UL13-deletion mutant in the PRV Becker background.
569 Further, we also used the Becker mutant, PRV 180 (which encodes the VP26- mRFP1 fusion
570 protein that is incorporated into capsids) to construct mutants with UL13 fused to enhanced green
571 fluorescence protein (eGFP). We also replaced the VP16 coding sequence with a hybrid gene
572 encoding a fusion protein with VP16 fused to mTurquoise v2 (mTurq) as internal control. We
573 showed that homologous recombination-mediated gene replacement was highly efficient upon
574 sgRNA/Cas9-nicking of target PRV DNA. Indeed, up to 83% of all progeny viruses formed
575 fluorophore-positive plaques. This percentage is similar or even higher than previously described
576 for the construction of PRV mutants through CRISPR/Cas9 (11, 12). However, these published
577 studies did not screen selected sgRNAs for potential off-target effects. Non-specific binding of
578 sgRNAs to genomic regions outside the target sequence can result in unwanted mutations in the
579 those genes (31). Therefore, we used the CRISPOR algorithm to select sgRNAs without any
580 potential off-target effects in the PRV genome (19).

581 Disruption of UL13 clearly reduced production of infectious virus, as PRV Δ UL13 produced a
582 10-fold lower viral titer compared to PRV WT at 18 hpi. This decrease was comparable to that
583 previously reported for two PRV mutants carrying UL13 deletions (29, 32). Also, the infectivity
584 and spread of PRV Δ UL13 in PK15 cells was decreased compared to PRV WT, as PRV Δ UL13
585 produced about 10-fold fewer plaques that were on average 1.5-fold smaller in diameter
586 compared to PRV WT. This phenomenon has already been described for other
587 alphaherpesviruses such as HSV-1 lacking UL13 (33). It was suggested that HSV-1 tegument
588 uncoating might be affected in absence of UL13 through lack of phosphorylation of viral
589 components, actin or other cytoskeletal elements (34). In addition, HSV-2 UL13 was proposed to
590 regulate nuclear egress by localized disruption of nuclear lamins (35). The latter hypothesis is
591 consistent with the perinuclear localization we observed for UL13, but especially for the fusion
592 protein UL13-eGFP. These data indicate that during virus propagation, UL13 accumulates close
593 to nuclear lamins and might be involved in nuclear egress of PRV. In absence of UL13, nuclear
594 egress of PRV and thus virus propagation might be affected. Still, the exact role of UL13 in the
595 infectivity and spread of PRV remains enigmatic.

596 As described for HSV-1 strain KVP26mRFP1 expressing a VP26 fusion with mRFP, the
597 replication of PRV 180 was decreased compared to the parental strain. This difference might be
598 caused by the steric hindrance of mRFP or a destabilization effect of fusion capsid proteins
599 during capsid formation. However, unlike disrupting UL13, fusing the kinase to eGFP did not
600 affect virus propagation kinetics, infectivity or spread. Indeed, the viral titers, number of plaques
601 and plaque diameters of PRV 180 UL13-eGFP did not significantly differ from those of its
602 parental strain, PRV 180. These data also suggest that tagging UL13 with eGFP does not
603 influence its (kinase) activity, as PRV Δ UL13 induced smaller plaques, while PRV UL13-eGFP

604 did not. The fact that PRV UL13-eGFP was still able to induce escape from silencing by PRV
605 virions destined for quiescence, while PRV Δ UL13 was not, corroborates this hypothesis.
606 Similarly, fusing mTurq to the N- or C-terminal end of VP16 did not decrease its infectivity, as
607 described previously (9). Finally, fusing UL13 to eGFP did not affect velocities of capsid
608 trafficking in SCG axons, as capsid transport velocities were similar for all fusion mutants and
609 parental virus. These velocities of capsid transport also corresponded to those previously
610 published for PRV 180 in chick embryo DRGs (9).

611 Further, our initial hypothesis was that during retrograde viral transport in axons, UL13 moves
612 separately from PRV nucleocapsids similar to what was described for VP16 (9). In our
613 hypothesis, PRV capsids would arrive at the nuclear pore before UL13, preventing the tegument
614 kinase from activating PRV genome transcription and thus favoring UL13 quiescence. However,
615 we observed that while VP16 separates from capsids and stays behind upon axonal inoculation of
616 SCG neuronal axons, at least some UL13 copies are co-transported with capsids during
617 retrograde transport in axons. Although we were unable to track live transport of UL13 using
618 eGFP fluorescence, we were able to detect UL13-eGFP by immunofluorescence staining. In this
619 way we observed that red capsids arriving in the M compartment still contain UL13-eGFP. We
620 were unable to visualize UL13-eGFP directly with antibodies to UL13, presumably because of
621 the low amount of UL13 incorporated in the virion. Indeed, even mass spectrometry was not
622 sensitive enough to detect UL13 in PRV virions (36). Still, Western blot and
623 immunofluorescence staining of purified PRV virions demonstrated that UL13 is structurally
624 incorporated into PRV virions. As a kinase enzyme, UL13 can be reused in multiple cycles,
625 which may explain why low concentrations of UL13 are incorporated into virions. Similarly,
626 Us3, another important serine/threonine-protein kinase is also co-transported with PRV capsids

627 during retrograde axonal infection (9). The authors suggested that these viral kinases facilitate
628 PRV capsid transport by stabilizing membrane-capsid and microtubule-capsid interactions.

629 The fact that UL13 is co-transported with PRV capsids, does not exclude its function in escape
630 from genome silencing by PRV. Indeed, we demonstrated that escape from genome silencing
631 indirectly requires viral tegument protein UL13. Following infection of neuronal cell bodies with
632 UV-inactivated PRV virions devoid of UL13, axonal PRV 180 infection was silenced. In
633 contrast, cell body infections with UV-inactivated PRV wild type virions enabled a productive
634 infection by axonally-transported PRV 180 particles. However, UL13 alone expressed in cell
635 bodies from AAV vectors was not sufficient to induce PRV genome silencing. It should be noted
636 that we were technically unable to verify the kinase activity of AAV-expressed UL13, as no such
637 tests are currently readily available. Still, our findings from the compartmentalization assays and
638 co-transport analyses suggest that UL13 is involved in PRV escape from genome silencing
639 through indirect mechanisms. We propose that another viral tegument protein, yet to be
640 identified, primes SCG neurons for productive axonal infection upon phosphorylation by UL13.
641 In absence of UL13, this tegument protein is not phosphorylated and thus remains inactive. For
642 HSV, UL13 has been suggested to phosphorylate glycoprotein E and I, UL41, Us3, ICP0, VP22
643 and ICP22 (34, 37-42). Glycoproteins E and I are embedded in the viral envelope and likely
644 remain at the plasma and/or endocytic membranes during virion entry. UL41 is a virion host shut
645 off endoribonuclease with no apparent effect on viral gene transcription, and the role of Us3 and
646 EP0 (orthologue of HSV ICP0) in PRV escape from silencing have already been ruled out (4,
647 43). Therefore, these proteins are unlikely to facilitate productive PRV infection in the
648 compartmentalization assay. In contrast, tegument proteins VP22 and ICP22 are interesting
649 candidates for further research. Major tegument protein VP22 of HSV-1 inhibits nucleosome

650 deposition on DNA by binding to TAF-I (template-activating factor I) and thereby activates viral
651 gene transcription (44). It may be that non-phosphorylated PRV VP22 is unable to recruit
652 histones to incoming PRV genomes and thus, trigger escape from silencing. PRV ICP22 is a
653 tegument protein important for proper PRV gene expression (45). Interestingly, HSV-1 ICP22 is
654 extensively phosphorylated and mediates, in conjunction with UL13, the phosphorylation of
655 RNA polymerase II (7, 42, 46). Perhaps this interplay between UL13 and ICP22 is also necessary
656 to induce escape from silencing. Finally, it is also possible that multiple proteins need to be
657 activated by UL13 phosphorylation in order to prevent genome silencing. Alternatively, UL13
658 might act in parallel with another tegument protein and both might be required for efficient
659 escape from genome silencing. Future studies, including the addition of UV-inactivated PRV
660 Δ UL13 to AAV-UL13 transduced cell bodies in trans and characterization of viral protein
661 phosphorylation profiles, will help to uncover the role of these tegument proteins.

662 In this report, we used CRISPR/Cas9-constructed PRV mutants and complementing AAV
663 transduction to show that UL13 is indirectly involved in PRV escape from genome silencing in
664 neurons. Accordingly, it may act through phosphorylation of other tegument proteins (e.g. VP22
665 or ICP22). Further, we showed that unlike VP16, UL13 remains with PRV capsids after axonal
666 entry and may mediate interactions between PRV capsids and cellular microtubules or
667 membranes. These new insights in alphaherpesvirus escape from quiescence will forward the
668 development of efficient antiviral therapies, a significant aspect of medical research on
669 herpesvirus-induced diseases.

670 **Acknowledgments**

671 The authors are grateful to all members of the Enquist lab and the Engel lab for their critical
672 comments on the project. We thank our many colleagues for sharing antibodies and reagents.

673 This research was supported by grants from the National Institutes of Health (NIH): RO1
674 NS33506 and NS060699. The funders had no role in study design, data collection and analysis,
675 decision to publish, or preparation of the manuscript.

676 The authors declare that the research was conducted in the absence of any commercial or
677 financial relationships that could be construed as a potential conflict of interest.

678 **References**

- 679 1. Grinde B. 2013. Herpesviruses: latency and reactivation – viral strategies and host
680 response. *Journal of Oral Microbiology* 5:10.3402/jom.v5i0.22766.
- 681 2. Roizman B, Zhou G. 2015. The 3 facets of regulation of herpes simplex virus gene
682 expression: A critical inquiry. *Virology* 479-480:562-567.
- 683 3. Whitley R KD, Prober CG. 2007. Pathogenesis and disease. In: Arvin A, Campadelli-
684 Fiume G, Mocarski E, et al., editors. *Human Herpesviruses: Biology, Therapy, and*
685 *Immunoprophylaxis*. Cambridge: Cambridge University Press; 2007. Chapter 32.
686 Available from: <https://www.ncbi.nlm.nih.gov/books/NBK47449/>.
- 687 4. Koyuncu OO, MacGibeny MA, Hogue IB, Enquist LW. 2017. Compartmented neuronal
688 cultures reveal two distinct mechanisms for alpha herpesvirus escape from genome
689 silencing. *PLoS Pathog* 13:e1006608.
- 690 5. Curanovic D, Ch'ng TH, Szpara M, Enquist L. 2009. Compartmented neuron cultures for
691 directional infection by alpha herpesviruses. *Curr Protoc Cell Biol* Chapter 26:Unit 26.4.
- 692 6. Koyuncu OO, Song R, Greco TM, Cristea IM, Enquist LW. 2015. The Number of
693 Alphaherpesvirus Particles Infecting Axons and the Axonal Protein Repertoire
694 Determines the Outcome of Neuronal Infection. *mBio* 6:e00276-15.
- 695 7. Long MC, Leong V, Schaffer PA, Spencer CA, Rice SA. 1999. ICP22 and the UL13
696 protein kinase are both required for herpes simplex virus-induced modification of the
697 large subunit of RNA polymerase II. *J Virol* 73:5593-604.
- 698 8. Jacob T, Van den Broeke C, Favoreel HW. 2011. Viral serine/threonine protein kinases.
699 *Journal of virology* 85:1158-1173.
- 700 9. Antinone SE, Smith GA. 2010. Retrograde Axon Transport of Herpes Simplex Virus and
701 Pseudorabies Virus: a Live-Cell Comparative Analysis. *Journal of Virology* 84:1504.
- 702 10. Hsu PD, Lander ES, Zhang F. 2014. Development and applications of CRISPR-Cas9 for
703 genome engineering. *Cell* 157:1262-78.
- 704 11. Liang X, Sun L, Yu T, Pan Y, Wang D, Hu X, Fu Z, He Q, Cao G. 2016. A CRISPR/Cas9
705 and Cre/Lox system-based express vaccine development strategy against re-emerging
706 Pseudorabies virus. *Scientific Reports* 6:19176.
- 707 12. Guo J-C, Tang Y-D, Zhao K, Wang T-Y, Liu J-T, Gao J-C, Chang X-B, Cui H-Y, Tian Z-
708 J, Cai X-H, An T-Q. 2016. Highly Efficient CRISPR/Cas9-Mediated Homologous
709 Recombination Promotes the Rapid Generation of Bacterial Artificial Chromosomes of
710 Pseudorabies Virus. *Frontiers in microbiology* 7:2110-2110.

- 711 13. Lin C, Li H, Hao M, Xiong D, Luo Y, Huang C, Yuan Q, Zhang J, Xia N. 2016.
712 Increasing the Efficiency of CRISPR/Cas9-mediated Precise Genome Editing of HSV-1
713 Virus in Human Cells. *Scientific Reports* 6:34531.
- 714 14. King MW, Munger J. 2019. Editing the human cytomegalovirus genome with the
715 CRISPR/Cas9 system. *Virology* 529:186-194.
- 716 15. Ch'ng TH, Flood EA, Enquist LW. 2005. Culturing primary and transformed neuronal
717 cells for studying pseudorabies virus infection. *Methods Mol Biol* 292:299-316.
- 718 16. Platt KB, Mare CJ, Hinz PN. 1979. Differentiation of vaccine strains and field isolates of
719 pseudorabies (Aujeszky's disease) virus: thermal sensitivity and rabbit virulence markers.
720 *Arch Virol* 60:13-23.
- 721 17. del Rio T, Ch'ng TH, Flood EA, Gross SP, Enquist LW. 2005. Heterogeneity of a
722 fluorescent tegument component in single pseudorabies virus virions and enveloped
723 axonal assemblies. *Journal of virology* 79:3903-3919.
- 724 18. Haeussler M, Schönig K, Eckert H, Eschstruth A, Mianné J, Renaud J-B, Schneider-
725 Maunoury S, Shkumatava A, Teboul L, Kent J, Joly J-S, Concordet J-P. 2016. Evaluation
726 of off-target and on-target scoring algorithms and integration into the guide RNA
727 selection tool CRISPOR. *Genome Biology* 17:148.
- 728 19. Concordet JP, Haeussler M. 2018. CRISPOR: intuitive guide selection for CRISPR/Cas9
729 genome editing experiments and screens. *Nucleic Acids Res* 46:W242-w245.
- 730 20. Chan KY, Jang MJ, Yoo BB, Greenbaum A, Ravi N, Wu WL, Sánchez-Guardado L, Lois
731 C, Mazmanian SK, Deverman BE, Gradinaru V. 2017. Engineered AAVs for efficient
732 noninvasive gene delivery to the central and peripheral nervous systems. *Nat Neurosci*
733 20:1172-1179.
- 734 21. Zolotukhin S, Byrne BJ, Mason E, Zolotukhin I, Potter M, Chesnut K, Summerford C,
735 Samulski RJ, Muzyczka N. 1999. Recombinant adeno-associated virus purification using
736 novel methods improves infectious titer and yield. *Gene Therapy* 6:973-985.
- 737 22. Maturana CJ, Verpeut JL, Pisano TJ, Dhanerawala ZM, Esteves A, Enquist LW, Engel
738 EA. 2020. Small Alpha herpesvirus Latency-Associated Promoters Drive Efficient and
739 Long-Term Transgene Expression in the CNS. *Mol Ther Methods Clin Dev* 17:843-857.
- 740 23. Tombácz D, Tóth JS, Petrovski P, Boldogkoi Z. 2009. Whole-genome analysis of
741 pseudorabies virus gene expression by real-time quantitative RT-PCR assay. *BMC*
742 *genomics* 10:491-491.
- 743 24. Wu BW, Engel EA, Enquist LW. 2014. Characterization of a Replication-Incompetent
744 Pseudorabies Virus Mutant Lacking the Sole Immediate Early Gene IE180. *mBio*
745 5:e01850-14.
- 746 25. MacGibeny MA, Koyuncu OO, Wirblich C, Schnell MJ, Enquist LW. 2018. Retrograde
747 axonal transport of rabies virus is unaffected by interferon treatment but blocked by
748 emetine locally in axons. *PLoS pathogens* 14:e1007188.
- 749 26. Olsen LM, Ch'ng TH, Card JP, Enquist LW. 2006. Role of pseudorabies virus Us3 protein
750 kinase during neuronal infection. *Journal of virology* 80:6387-6398.
- 751 27. Taylor MP, Kratchmarov R, Enquist LW. 2013. Live cell imaging of alpha herpes virus
752 anterograde transport and spread. *J Vis Exp* doi:10.3791/50723.
- 753 28. Granstedt AE, Brunton BW, Enquist LW. 2013. Imaging the Transport Dynamics of
754 Single Alpha herpesvirus Particles in Intact Peripheral Nervous System Explants from
755 Infected Mice. *mBio* 4:e00358-13.

- 756 29. Coller KE, Smith GA. 2008. Two viral kinases are required for sustained long distance
757 axon transport of a neuroinvasive herpesvirus. *Traffic (Copenhagen, Denmark)* 9:1458-
758 1470.
- 759 30. Klopffleisch R, Klupp BG, Fuchs W, Kopp M, Teifke JP, Mettenleiter TC. 2006. Influence
760 of Pseudorabies Virus Proteins on Neuroinvasion and Neurovirulence in Mice. *Journal of*
761 *Virology* 80:5571.
- 762 31. Zhang X-H, Tee LY, Wang X-G, Huang Q-S, Yang S-H. 2015. Off-target Effects in
763 CRISPR/Cas9-mediated Genome Engineering. *Molecular Therapy - Nucleic Acids*
764 4:e264.
- 765 32. de Wind N, Domen J, Berns A. 1992. Herpesviruses encode an unusual protein-
766 serine/threonine kinase which is nonessential for growth in cultured cells. *Journal of*
767 *virology* 66:5200-5209.
- 768 33. Gershburg S, Geltz J, Peterson KE, Halford WP, Gershburg E. 2015. The UL13 and US3
769 Protein Kinases of Herpes Simplex Virus 1 Cooperate to Promote the Assembly and
770 Release of Mature, Infectious Virions. *PLoS One* 10:e0131420.
- 771 34. Morrison EE, Wang YF, Meredith DM. 1998. Phosphorylation of structural components
772 promotes dissociation of the herpes simplex virus type 1 tegument. *Journal of virology*
773 72:7108-7114.
- 774 35. Cano-Monreal GL, Wylie KM, Cao F, Tavis JE, Morrison LA. 2009. Herpes simplex
775 virus 2 UL13 protein kinase disrupts nuclear lamins. *Virology* 392:137-47.
- 776 36. Kramer T, Greco TM, Enquist LW, Cristea IM. 2011. Proteomic characterization of
777 pseudorabies virus extracellular virions. *Journal of virology* 85:6427-6441.
- 778 37. Ogle WO, Ng TI, Carter KL, Roizman B. 1997. The UL13 protein kinase and the infected
779 cell type are determinants of posttranslational modification of ICP0. *Virology* 235:406-
780 13.
- 781 38. Ng TI, Ogle WO, Roizman B. 1998. UL13 protein kinase of herpes simplex virus 1
782 complexes with glycoprotein E and mediates the phosphorylation of the viral Fc receptor:
783 glycoproteins E and I. *Virology* 241:37-48.
- 784 39. Asai R, Ohno T, Kato A, Kawaguchi Y. 2007. Identification of proteins directly
785 phosphorylated by UL13 protein kinase from herpes simplex virus 1. *Microbes and*
786 *infection* 9:1434-1438.
- 787 40. Overton H, McMillan D, Hope L, Wong-Kai-In P. 1994. Production of Host Shutoff-
788 Defective Mutants of Herpes Simplex Virus Type 1 by Inactivation of the UL13 Gene.
789 *Virology* 202:97-106.
- 790 41. Kato A, Yamamoto M, Ohno T, Tanaka M, Sata T, Nishiyama Y, Kawaguchi Y. 2006.
791 Herpes Simplex Virus 1-Encoded Protein Kinase UL13 Phosphorylates Viral Us3 Protein
792 Kinase and Regulates Nuclear Localization of Viral Envelopment Factors UL34 and
793 UL31. *Journal of Virology* 80:1476.
- 794 42. Purves FC, Roizman B. 1992. The UL13 gene of herpes simplex virus 1 encodes the
795 functions for posttranslational processing associated with phosphorylation of the
796 regulatory protein alpha 22. *Proc Natl Acad Sci U S A* 89:7310-4.
- 797 43. Jiang Z, Su C, Zheng C. 2016. Herpes Simplex Virus 1 Tegument Protein UL41
798 Counteracts IFIT3 Antiviral Innate Immunity. *Journal of Virology* 90:11056.
- 799 44. van Leeuwen H, Okuwaki M, Hong R, Chakravarti D, Nagata K, O'Hare P. 2003. Herpes
800 simplex virus type 1 tegument protein VP22 interacts with TAF-I proteins and inhibits
801 nucleosome assembly but not regulation of histone acetylation by INHAT. *J Gen Virol*
802 84:2501-2510.

- 803 45. Takács IF, Tombácz D, Berta B, Prazsák I, Póka N, Boldogkői Z. 2013. The ICP22
804 protein selectively modifies the transcription of different kinetic classes of pseudorabies
805 virus genes. BMC molecular biology 14:2-2.
- 806 46. Lin F-s, Ding Q, Guo H, Zheng AC. 2010. The herpes simplex virus type 1 infected cell
807 protein 22. Virologica Sinica 25:1-7.

808 **Figure captions**

809 **Figure 1**

810 CRISPR/Cas9-mediated mutagenesis of PRV through homology-directed recombineering of the
811 PRV genome. (A) Schematic of *UL13*- and *VP16*-targeting and *eGFP* or *mTurq* incorporation.
812 (B) Workflow of PRV mutant production. (C) Efficacy of (fluorescent) progeny virus
813 propagation in HEK293T cells with or without stable expression of sgRNA-Cas9 upon
814 transfection of whole PRV genome, inoculation by PRV virions and/or addition of donor
815 plasmids. Three independent experiments were performed, and data are represented as means +
816 SD. Different lower case letters indicate significant ($P<0.05$) differences in the total number of
817 plaques among different experimental conditions. Different upper case letters indicate significant
818 ($P<0.05$) differences in the number of fluorescent plaques among different experimental
819 conditions.

820 **Figure 2**

821 Characterization of newly constructed PRV mutants. All scale bars represent 100 μm . (A)
822 Fluorescence microscopy images of PRV wild type (WT) and PRV ΔUL13 plaques in PK15
823 cells. (B) Fluorescence microscopy images of PRV 180, PRV 180 UL13-eGFP, PRV 180 mTurq-
824 VP16 and PRV 180 VP16-mTurq plaques in PK15 cells. Magnified images (3X) of the green or
825 blue channels are shown in the lower right corner of the respective images. (C) Absence of UL13
826 in PRV ΔUL13 was confirmed by immunofluorescence staining using polyclonal rabbit anti-
827 UL13 antibodies. (D) Co-localization of eGFP with UL13 and mTurq with VP16 in PRV 180

828 UL13-eGFP and PRV 180 mTurq-VP16 or PRV 180 VP16-mTurq, respectively, as conformed
829 by immunofluorescence staining using polyclonal rabbit anti-UL13 or -VP16 antibodies. (E)
830 Western blot analysis of purified progeny virions (upper image). Agarose gel electrophoresis of
831 VP16 gene PCR products of different PRV strains (lower image).

832 **Figure 3**

833 Viral infectivity, spread and propagation parameters of newly constructed PRV mutants in PK15
834 cells. (A) Total number of plaques (left) and average plaque diameter (right) were determined 48
835 hpi upon standardizing the inoculum at 10^6 genome copies. Experiments were performed in
836 triplicate. Data are represented as means + SD and different lower case letters indicate significant
837 ($P < 0.05$) differences between different viral mutants. (B) Temporal virus propagation was
838 determined on PK15 cells by standardizing the inoculum at a MOI of 1. Significant differences
839 are indicated by asterisks: ***, $P < 0.001$. (C) Expression kinetics of different viral proteins were
840 determined on PK15 cells by immunofluorescence staining using antibodies against IE180
841 (immediate early protein), UL13 (viral kinase and tegument protein), Us3 (viral kinase and
842 tegument protein), VP16 (tegument protein), gB (envelope protein) and VP26 (capsid protein).
843 Experiments were performed in triplicate. Significant differences are indicated by asterisks: **,
844 $P < 0.01$; ***, $P < 0.001$.

845 **Figure 4**

846 Validation of PRV 180 UL13-eGFP and PRV 180 mTurq-VP16 for live cell imaging. Red
847 particles (mRFP1-capsid) from purified viral stocks were analyzed for green (PRV 180 UL13-
848 eGFP) and cyan (PRV 180 mTurq-VP16) fluorescence emission. PRV 180 UL13-eGFP were
849 additionally stained with polyclonal rabbit anti-eGFP antibodies. Pie charts show the proportion

850 of virions with structurally incorporated UL13 or VP16 (dual fluorescent) to capsids without
851 UL13 or VP16 incorporation (mono fluorescent). Scale bars represent 10 μm .

852 **Figure 5**

853 Axonal transport of UL13 and VP16 in compartmented SCG neurons. All scale bars represent 10
854 μm . (A) Live-cell imaging of PRV 180, PRV 180 UL13-eGFP and PRV 180 mTurq-VP16
855 retrograde transport (see also Movie 1-3). Images show the merge of red, green and phase of a
856 Movie snapshot. Pie charts show the proportion of moving mono or dual fluorescent capsids to
857 mono or dual fluorescent stationary capsids. Capsid velocities are given in the graph.
858 Experiments were performed in triplicate. Different lower case letters represent significant
859 differences ($P < 0.05$). (B) Immunofluorescence staining of eGFP in M (left) and N (right)
860 compartment 2 hpi to track UL13 transport in combination with capsid transport. Pie charts show
861 the proportion of dual fluorescent capsids to mono fluorescent capsids. Arrows and arrowheads
862 point at mono and dual fluorescent capsids, respectively.

863 **Figure 6**

864 UL13 is important in the escape from genome silencing by PRV. (A) Schematic of
865 complementation assay used to study escape from genome silencing in chambered SCG neurons.
866 (B) Phase, fluorescent and merged images of S compartments 4 days pi using different stimuli in
867 the S compartment. DiO was added to the N compartment to visualize the number of neurons
868 with N compartment-penetrating axons. Scale bars represent 1000 μm . (C) The percentage of
869 PRV capsid-positive neurons on the total number of neurons with N compartment-penetrating
870 axons. Experiments were performed 5 times. Data are shown as mean + SD and significant
871 differences ($P < 0.05$) are indicated by different lower case letters.

872 **Figure 7**

873 UL13 is not directly involved in the escape from genome silencing by PRV. (A) SCG neuronal
 874 bodies express eGFP and/or UL13 6 days upon inoculation by AAV vectors. (B) Phase,
 875 fluorescent and merged images of S compartments 4 days pi following AAV-induced
 876 UL13/eGFP expression in the S compartment. Scale bars represent 1000 μ m. (C) The percentage
 877 of PRV capsid-positive neurons on the total number of neurons. Experiments were performed 5
 878 times. Data are shown as mean + SD and significant differences ($P < 0.05$) are indicated by
 879 different lower case letters.

880 **Tables**881 **Table 1. CRISPR/Cas9 target sequences**

Name	spCas9 sgRNA + <u>PAM</u>	Target sequences (GenBank JF797219.1)
UL13 sgRNA	cgaggccgtcatgacgctgc <u>TGG</u>	77651-77673
VP16 sgRNA 1	gtgcgtggtcgcttcgacg <u>AGG</u>	9978-10000
VP16 sgRNA 2	acatccggtgagcgcgtcg <u>CGG</u>	11172-11194

882

883 **Table 2. Fragment and primer design for HiFi DNA assembly**

884 Silent mutations (underlined> were introduced in PAM sequences of PRV 180 fusion mutants.

	Name	Length (bp)	Primer design (5'-3')	
			Forward	Reverse
UL13 deletion donor plasmid	Vector backbone	5420	cggttctg- TCTAGAGGGCCCTATTC TATAG	ctttccatc- TGTGATGGATATCTGCAG
	Upfront homology arm	609	atccatcaca- GATGGCAAAGTTGAAA AAGCGGGC	cggccgccag- TCACGCCTCCTCCGCTC
	eGFP	756	ggaggegtga- CTGGCGCCGCTCGAGA T	gcgcgccat- TTACTTGTACAGCTCGTCC ATGCCG
	Downstream homology arm	875	gtacaagtaa- ATGGCGGCGCTCGTTTT GC	gccctctaga- CAGGAACCCGCGCAGCGT
UL13 -GFP	Vector backbone	5420	ggaggagctg- TCTAGAGGGCCCTATTC TATAG	cgccataaag- TGTGATGGATATCTGCAG

	Upfront homology arm	650	atccatcaca-CTTTATGGCGGCCAAACAGG	tgctcacat-GAGCGTCTTCACGGCCAC
	eGFP	737	gaagacgctc-ATGGTGAGCAAGGGCGAG	agccggcgcg-CTTGTACAGCTCGTCCATGC
	Downstream homology arm	764	gctgtacaag-CGCGCCGGCTTCGGACA	gccctctaga-CAGCTCCTCCTCGAGGATGTCCCC
mTurq-VP16 fusion donor plasmid	Vector backbone	5420	gtcgaggagc-TCTAGAGGGCCCTATCTATAG	tcgagctgga-TGTGATGGATATCTGCAG
	Upfront homology arm	821	atccatcaca-TCCAGCTCGAGAAAGACCCGG	tgctcacat-CCTCACCGACCCCCCAC
	mTurq	737	gtcggtagg-ATGGTGAGCAAGGGCGAG	cgtegcgcat-CTTGTACAGCTCGTCCATGC
	Downstream homology arm	873	gctgtacaag-ATGCGCGACGAGGAGTGCGTGGTCGCGTTTCGACGAA	gccctctaga-GCTCCTCGACCAGGTTCGG
VP16-mTurq fusion donor plasmid	Vector backbone	5420	gactacctgt-TCTAGAGGGCCCTATCTATAG	aagaagcgt-TGTGATGGATATCTGCAG
	Upfront homology arm	874	atccatcaca-AGCGCTTCTTCGTGTCCAC	tggcgaccgg-CATCTCAAACATCCIGTTGAG
	mTurq	752	gtttgagatg-CCGGTCGCCACCATGGTG	gcgcgggcg-TTACTTGTACAGCTCGTCCATGCC
	Downstream homology arm	595	gtacaagtaa-CGCCGCGCGCGGTTCGGA	gccctctaga-ACAGGTAGTCCACGTCGGCGGG
AAV-eGFP	Vector backbone	4325	cggtcctga-AAGCTTATCGATAATCAACCTCTGG	tgctcacat-GCTAGCGGATCTGACGGTTC
	eGFP	641	atccgctagc-ATGGTGAGCAAGGGCGAG	ctttgctcag-GGCGGACTGGGTGCTCAG
	eGFP-p2a	185	ccagtccgcc-CTGAGCAAAGACCCCAA	cgataagctt-TCAAGGACCGGGGTTTTC
AAV-UL13	Vector backbone	4325	cgctgcctga-AAGCTTATCGATAATCAACCTCTGG	tgctcacat-GCTAGCGGATCTGACGGTTC
	eGFP	641	atccgctagc-ATGGTGAGCAAGGGCGAG	ctttgctcag-GGCGGACTGGGTGCTCAG

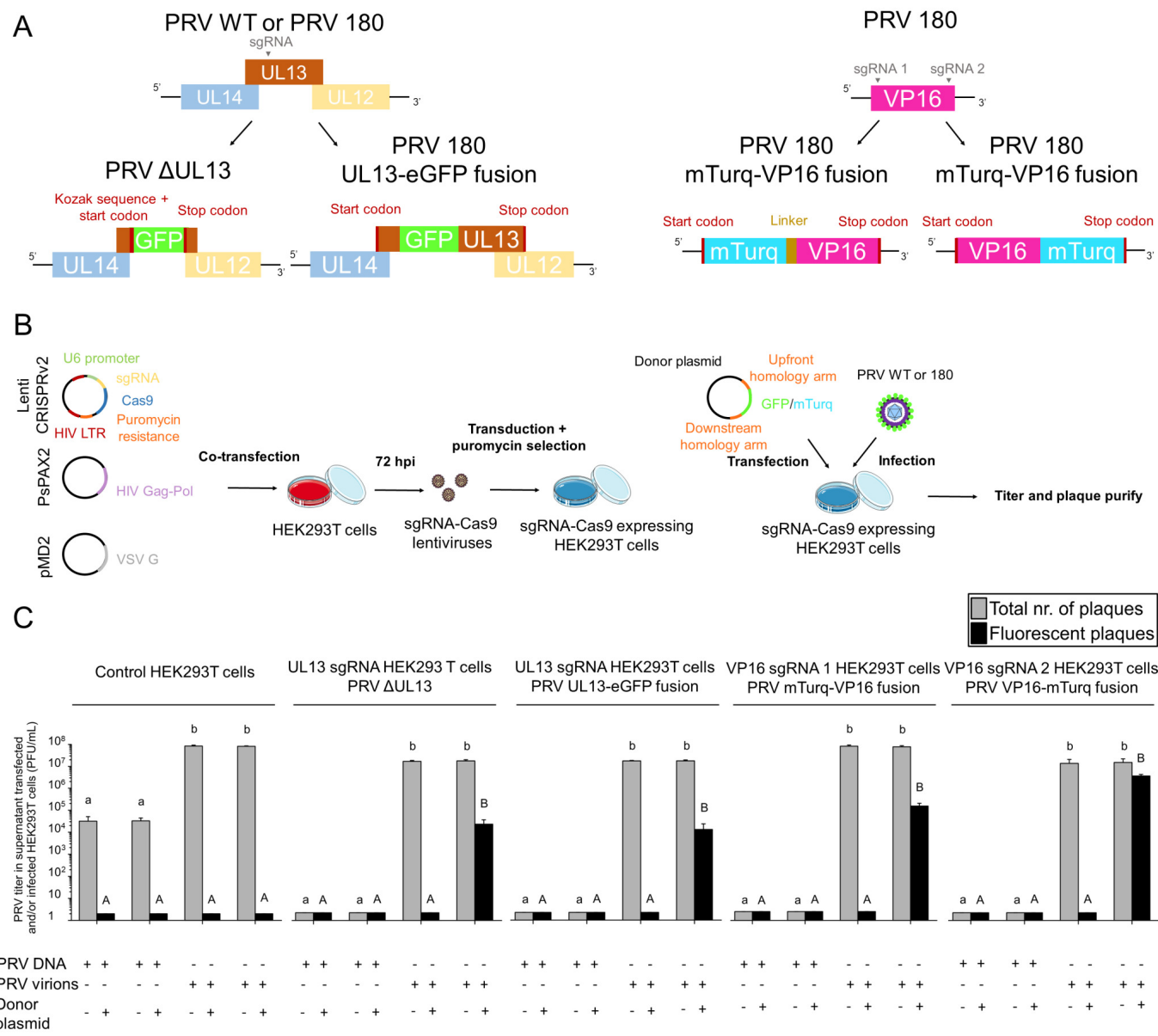
eGFP-p2a	182	ccagtccgcc- CTGAGCAAAGACCCCAA C	cagcagccat- AGGACCGGGGTTTTCTTC
UL13	1217	ccccggtctt- ATGGCTGCTGGAGGAGG C	cgataagctt- TCAGGCAGCGAGTTCGGC

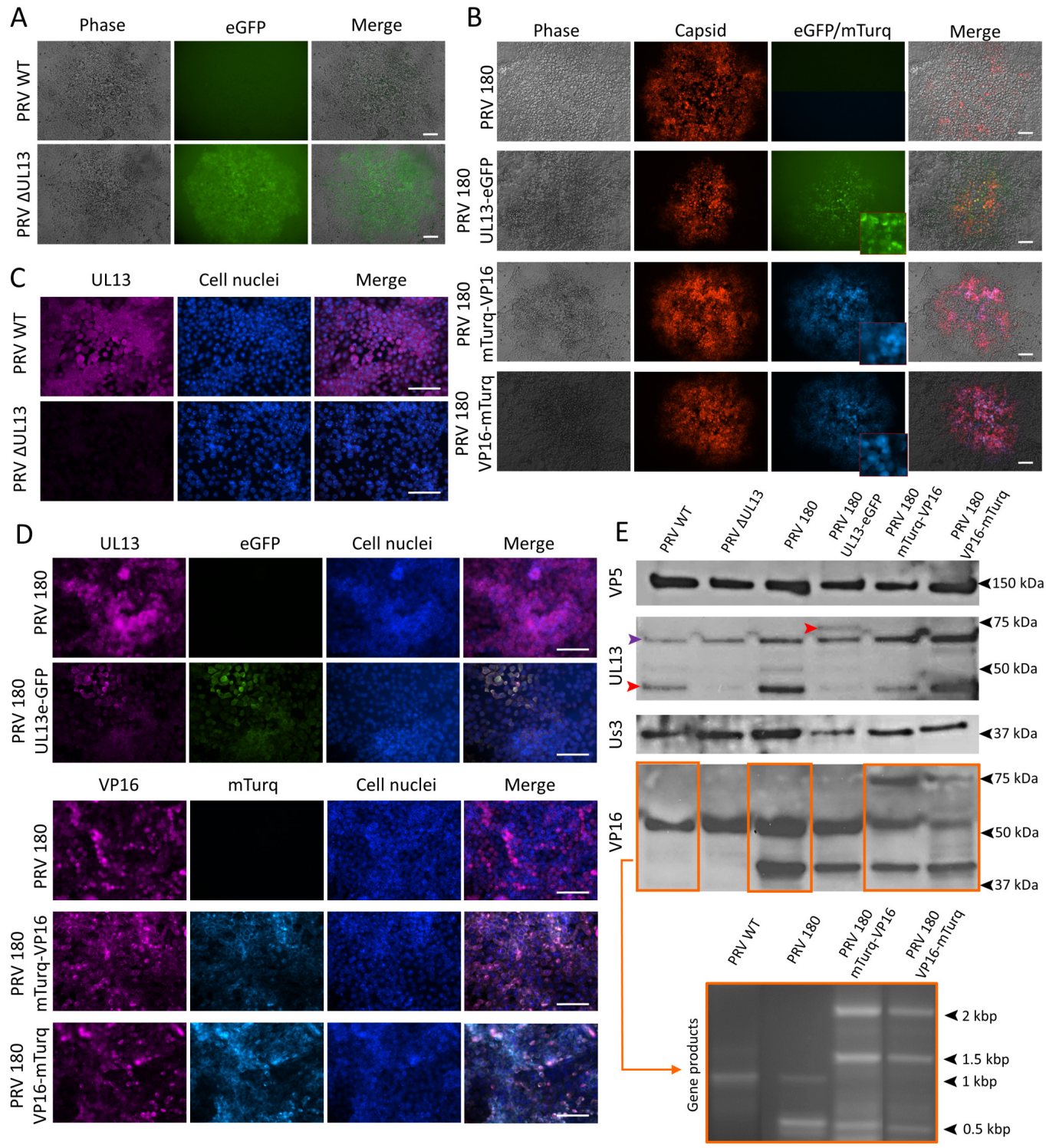
885

886 **Table 3. Primers for (q)PCR and sequencing**

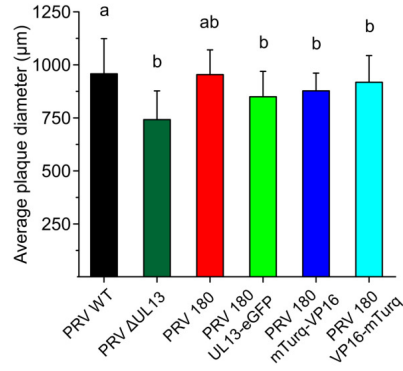
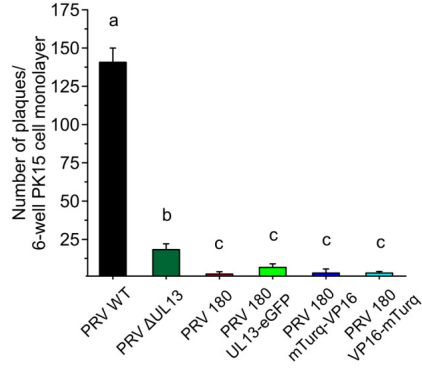
Name	Forward (5'-3')	Reverse (5'-3')
UL13 seq	gacgacgcggccgcgctcgacgaggac	ctcgacgagcaggtcgtgcacgtac
VP16 seq	ggacgagagcaccgccggcgaag	ccgcgtcgctcatggtggtcgctg
UL54 qPCR	tgcagctacacctcgtcc	tcaaacaggtggttcagtaaa

887

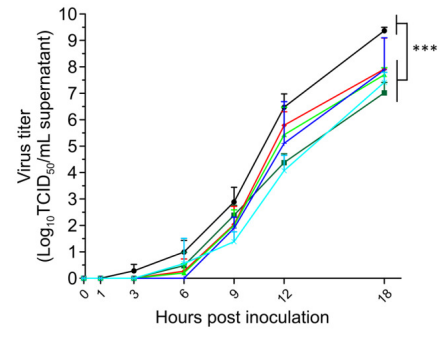




A



B



C

